PHYSICAL REVIEW B **85**, 020405(R) (2012)

Monte Carlo and variational calculations of the magnetic phase diagram of $CuFeO_2$

Randy S. Fishman,[1] Gregory Brown,[2] and Jason T. Haraldsen[3,4]

[1]*Materials Science and Technology Division, Oak Ridge National Laboratory, Oak Ridge, Tennessee 37831, USA*

[2]*Department of Physics, Florida State University, Tallahassee, Florida 32306, USA*

[3]*Theoretical Division, Los Alamos National Laboratory, Los Alamos, New Mexico 87545, USA*

[4]*Center for Integrated Nanotechnologies, Los Alamos National Laboratory, Los Alamos, New Mexico 87545, USA*

(Received 8 November 2011; published 12 January 2012)

Monte-Carlo and variational calculations are used to revise the phase diagram of the magnetically frustrated material $CuFeO_2$. For fields $50 < H < 65$T, a new spin-flop phase is predicted between a canted 3-sublattice phase and the conventional conical spin-flop phase. With wave vector $\mathbf{Q} \approx (0.8\pi, 0.43\pi)$, this phase is commensurate in the x direction but incommensurate in the y direction. A canted 5-sublattice phase is predicted between the multiferroic phase and either a collinear 5-sublattice phase for pure $CuFeO_2$ or a canted 3-sublattice phase for Al- or Ga-doped $CuFeO_2$.

DOI: 10.1103/PhysRevB.85.020405 PACS number(s): 75.10.Hk, 75.30.Kz, 75.50.Ee

Magnetic phase diagrams play a central role in understanding magnetic materials with competing interactions. Because competing phases lie close in energy, magnetically frustrated materials can exhibit remarkably complex phase diagrams. Several interesting materials with simple collinear (CL) ground states develop noncollinear (NC) states displaying multiferroic behavior upon either doping or applying a magnetic field.[1]

For both pure $MnWO_4$ (Ref. 2) and $CuFeO_2$ (Ref. 3), easy-axis anisotropy stabilizes CL spin states in a zero field. Nonmagnetic impurities or magnetic fields transform those CL states into distorted spirals that exhibit spontaneous electric polarizations.[4–7] Recently, Ref. 8 employed a variational technique to construct the phase diagram of doped $CuFeO_2$. Using classical Monte-Carlo (MC) simulations together with spin-wave and variational calculations, we now revise that phase diagram and predict a new spin-flop (SF) phase above 50 T.

Below 7 T, the observed ground state of pure $CuFeO_2$ is the 4-sublattice (SL) CL state sketched in Fig. 1(b). A complex NC (CNC) state with ferroelectric polarization appears between 7 and 13 T (Ref. 4). The CNC state is also stabilized by either Al (Refs. 5 and 6) or Ga (Refs. 9 and 10) doping. Inelastic neutron-scattering measurements were recently used[11] to characterize the multiferroic state of Ga-doped $CuFeO_2$ as a distorted spiral with alternating small ($\sim 22^\circ$) and large ($\sim 134^\circ$) turn angles $\Delta\theta$.

Between 13 and 20 T, Mitsuda *et al.*[12] observed the 5-SL phase sketched in Fig. 1(d) with normalized magnetization $M = \langle S_{iz}\rangle/S = 1/5$. At 20 T, the 5-SL phase transforms into the 3-SL phase sketched in Fig. 1(b) with $M = 1/3$; at 34 T, the 3-SL phase smoothly changes into a canted phase.[13] A weakly first-order transition into another canted phase was observed at 50 T (Refs. 14 and 15) and saturation into the completely aligned CL-1 state with $M = 1$ was reported at 70 T (Ref. 16).

Due to hysteresis, the first-order transitions from the CNC to the 5-SL phase and from the 5-SL to the 3-SL phase are poorly characterized. It is possible that intermediate phases lie between the CNC and 5-SL phases and between the 5-SL and 3-SL phases. In the nonstoichiometric compound $CuFeO_{2+\delta}$, Hasegawa *et al.*[17] observed an unspecified phase linking the 5-SL and 3-SL phases, which were separated by 3 T.

Because the hexagonal planes of $CuFeO_2$ are coupled antiferromagnetically, magnetic frustration only affects each hexagonal plane. Consequently, the magnetic phase diagram of $CuFeO_2$ can be constructed based on a two-dimensional model with interactions J_n that extend up to third nearest neighbors, as shown in Fig. 1(b). Since single-ion anisotropy D aligns the spins along the z axis for pure $CuFeO_2$ in low fields, the qualitative behavior of $CuFeO_2$ is described by the energy

$$E = -\frac{1}{2}\sum_{i\neq j} J_{ij}\mathbf{S}_i\cdot\mathbf{S}_j - D\sum_i {S_{iz}}^2 - 2\mu_B H\sum_i S_{iz}, \quad (1)$$

where the field $\mathbf{H}$ is applied along the z axis. Due to the large $S = 5/2$ spins of the Fe^{3+} ions, we have assumed that $\mathbf{S}_i \equiv \mathbf{S}(\mathbf{R}_i)$ are classical spins.

For a given set of exchange interactions $\{J_1 < 0, J_2, J_3\}$ and for Ising spins ($D \gg |J_n|$), Takagi and Mekata[18] constructed the possible CL ground states of E in a zero field. The 4-SL phase is stable in the region of phase space sketched in Fig. 1(a) with $J_3 < J_2/2$ and $-1/2 < J_2/|J_1| < 0$.

Earlier work[8] employed a variational approach to evaluate the phase diagram of Eq. (1). The spin state of the multiferroic CNC phase was expanded[19,20] in harmonics of the fundamental ordering wave vector $\mathbf{Q} = Q_C\,\mathbf{x}$:

$$S_z(\mathbf{R}) = \sum_{l=0}^{\infty} C_l\cos(l\,Q_C\,x), \quad (2)$$

$$S_y(\mathbf{R}) = \sqrt{S^2 - S_z(\mathbf{R})^2}\,\mathrm{sgn}(\sin(Q_C\,x)), \quad (3)$$

where the lattice constant was set to 1. The condition $\max|S_z(\mathbf{R})| = S$ was used to fix C_0. Because only terms up to C_5 were significant, the trial incommensurate spin state had six variational parameters (Q_C and C_l with $0 < l \leqslant 5$). The energy E was then minimized on a unit cell of length 10^4 with open boundary conditions.

With decreasing anisotropy (corresponding to increasing Al or Ga doping), the 4-SL CL phase eventually transforms into the CNC phase in zero field.[21] For region CL-4i of Fig. 1(a), the wave vector Q_C of the CNC phase depends on the parameters $\{J_2/|J_1|, J_3/|J_1|\}$. This region is believed to describe $CuFeO_2$. For region CL-4ii of Fig. 1(a), $Q_C = 4\pi/3$ is independent of the parameters $\{J_2/|J_1|, J_3/|J_1|\}$. This region is believed to

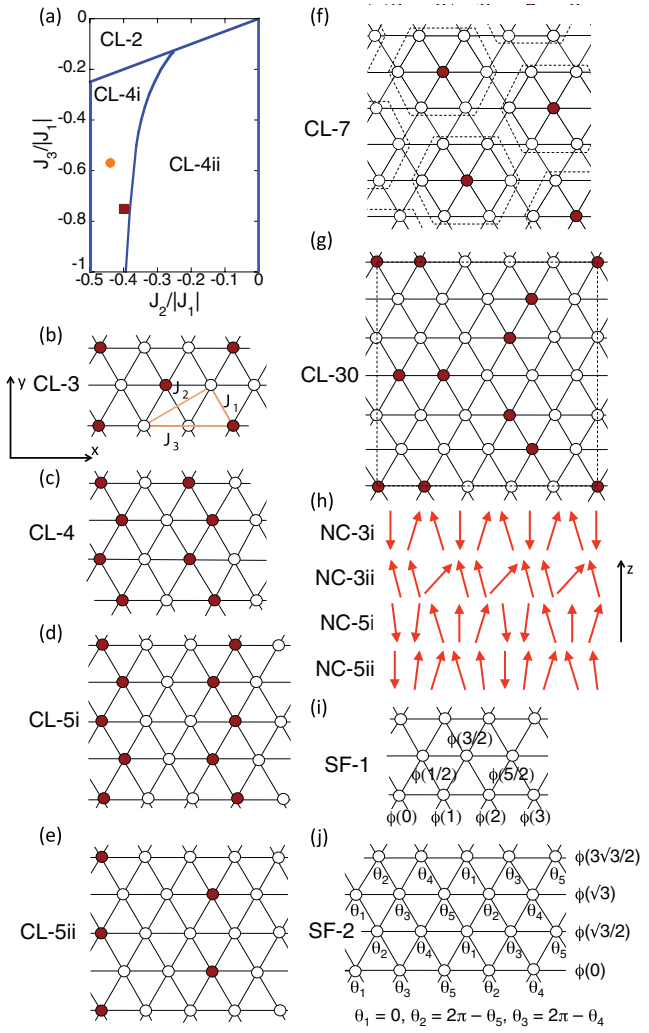

FIG. 1. (Color online) (a) The region of $\{J_2/|J_1|, J_3/|J_1|\}$ phase space supporting the CL-4 phase in a zero field for large anisotropy. Circular and square points indicate the parameters used to evaluate the phase diagrams in Figs. 2(a) and 2(b), respectively. (b) The CL-3 phase with exchange interactions J_n indicated. Other CL phases are the (c) CL-4, (d) CL-5i, (e) CL-5ii, (f) CL-7, and (g) CL-30 phases with open or closed circles indicating up or down spins, respectively, and dashed lines surrounding the unit cells in the last two cases. (h) The NC phases with 3 and 5 SLs, and (i) the SF-1 and (j) SF-2 phases.

describe $CuCrO_2$ (Ref. 22). The zero-field state in this region is more simply described as the NC-3i state sketched in Fig. 1(h) with $M < 1/3$.

To construct the magnetic phase diagram, Ref. 8 considered canted coplanar states with up to 10-SLs. A trial spin state was introduced for the conical SF phase pictured in Fig. 1(i). The SF-1 phase can be written $\mathbf{S}(\mathbf{R}) = S(\sin\theta\cos\phi(\mathbf{R}), \sin\theta\sin\phi(\mathbf{R}), \cos\theta)$ where the tilting angle θ is constant but the azimuthal angle $\phi(\mathbf{R}) = Q_1 x$ varies linearly with x. Hence, the SF-1 state has wave vector $\mathbf{Q} = (Q_1, 0)$ and two variational parameters (Q_1 and θ).

The phase diagram constructed in Ref. 8 contained three different canted 5-SL phases. However, the second of the canted 5-SL phases[23] was later discovered to be locally unstable with imaginary spin-wave frequencies for some wave vectors. In order to clarify the phase diagram of $CuFeO_2$, we have employed MC simulations for classical spins on a 60×60 lattice with periodic boundary conditions. Thermal annealing was used to search for ground states at selected points throughout the phase diagram for a given set of exchange interactions $\{J_2/|J_1|, J_3/|J_1|\}$.

Spin-wave calculations were used to verify that each of the MC states is locally stable. NC states were treated using the $1/S$ formalism described in Ref. 24. Based on the set of MC ground states, variational calculations were used to efficiently complete the phase diagram. Note that the MC states are only used to provide candidates whose energies are then evaluated either exactly (for CL states) or on a large lattice within a variational analysis (for NC states). Therefore, the finite-size limitations of the MC simulations are not critical. We are now convinced that the combination of MC simulations, spin-wave calculations, and variational techniques provides the most reliable and efficient way to construct the magnetic phase diagram of a system with competing interactions.

Aside from the CNC and CL-1 phases, the spin states found by MC simulations are described in Figs. 1(b) to 1(j). Compared to Ref. 8, MC simulations have revealed two additional CL phases. The CL-7 phase with $M = 5/7$ described in Fig. 1(f) is constructed by filling a triangular lattice with hexagons, each containing one down spin at its center. The CL-30 phase with $M = 7/15$ is described in Fig. 1(g). The energies and magnetizations of all CL phases are summarized in Table I, where $h \equiv 2\mu_B H/S|J_1|$.

Both canted 3-SL phases NC-3i and NC-3ii appeared in the phase diagram of $CuCrO_2$ (Ref. 22). Replacing the unstable canted 5-SL phase[23] from Ref. 8 is the new SF phase described in Fig. 1(j). Like the NC-5i state, the SF-2 state has a 5-SL period along the x axis with tilting angles $\theta_1 = 0$, $\theta_2 = 2\pi - \theta_5$, and $\theta_3 = 2\pi - \theta_4$. Unlike the NC-5i state, however, the SF-2 state is incommensurate along the y axis with azimuthal angle $\phi(\mathbf{R}) = Q_2\, y$, wave vector $\mathbf{Q} = (0.8\pi, Q_2)$, and three variational parameters (Q_2, θ_2, and θ_3).

Using the same parameters $\{J_2/|J_1|, J_3/|J_1|\} = \{-0.44, -0.57\}$ as in Ref. 8 [indicated by the circle in Fig. 1(a)], the revised phase diagram is plotted in Fig. 2(a). For fields $h > 4$, this phase diagram differs significantly from the earlier one, in particular because most of the phase space previously allotted to the SF-1 phase is now occupied by the SF-2 phase. In addition, the CL-30 phase now occupies most of the phase space previously allotted to the CL-3 phase. Due to the much diminished CL-3 phase, the phase diagram of Fig. 2(a) does not describe the measurements in $CuFeO_2$.

TABLE I. Energies and net spins of the CL states

Phase	E/NS^2	M
CL-1	$-3(J_1 + J_2 + J_3) - D - \lvert J_1\rvert h$	1
CL-3	$J_1 - 3J_2 + J_3 - D - \lvert J_1\rvert h/3$	1/3
CL-4	$J_1 - J_2 + J_3 - D$	0
CL-5i	$(J_1 + J_2)/5 + J_3 - D - \lvert J_1\rvert h/5$	1/5
CL-5ii	$-3(J_1 + J_3)/5 - 7J_2/5 - D - 3\lvert J_1\rvert h/5$	3/5
CL-7	$-9(J_1 + J_3 + J_3)/7 - D - 5\lvert J_1\rvert h/7$	5/7
CL-30	$-J_1/3 - 3J_2/5 + J_3/5 - D - 7\lvert J_1\rvert h/15$	7/15

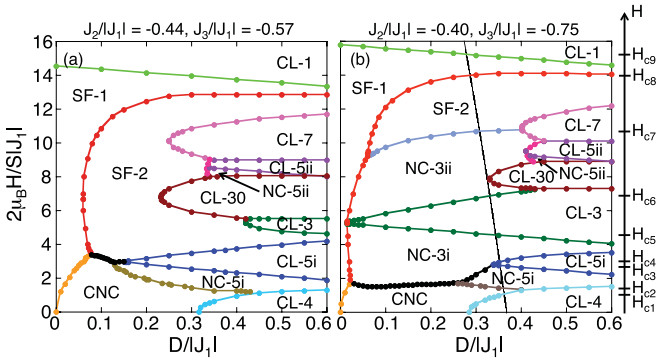

FIG. 2. (Color online) Magnetic phase diagrams as a function of the external field and anisotropy for two different sets of parameters. A possible trajectory through the second phase diagram for $CuFeO_2$ is given by the thin curve with critical fields indicated on the right-hand side.

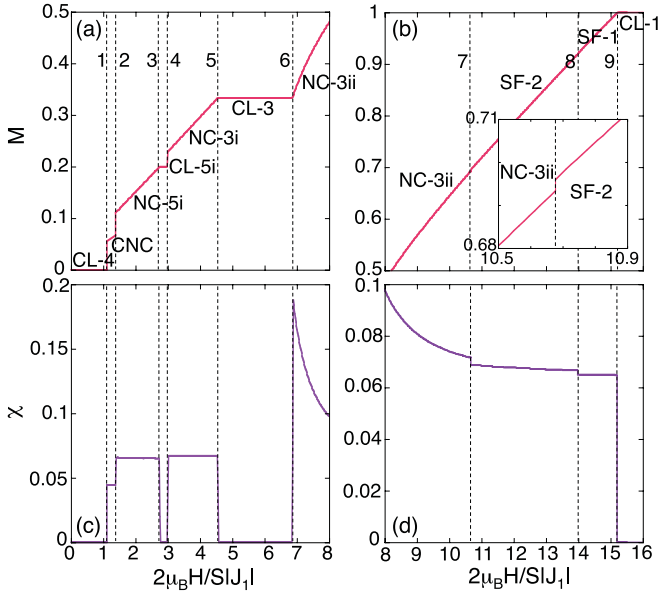

FIG. 3. (Color online) (a), (b) Magnetization M and (c), (d) susceptibility $\chi = dM/dh$ vs field $h = 2\mu_B H/S|J_1|$ for $J_2/|J_1| = -0.40$ and $J_3/|J_1| = -0.75$. The trajectory plotted in Fig. 2(b) contains the nine critical fields indicated by the dashed vertical lines.

However, the CL-3 phase is significantly enlarged by shifting the exchange parameters closer to the CL-4i/CL-4ii boundary. The phase diagram for $\{J_2/|J_1|, J_3/|J_1|\} = \{-0.40, -0.75\}$ [indicated by the square in Fig. 1(a)] is plotted in Fig. 2(b). Both sets of parameters in Fig. 2 produce CNC phases with $Q_C \approx 0.85\pi$ when $D = 0$. The phase diagram of Fig. 2(b) now includes NC-3i and NC-3ii phases on either side of a much more prominent CL-3 phase. Both the CL-5 and CNC phases in Fig. 2(b) occupy a much smaller region of phase space than in Fig. 2(a). The CNC phase with a variable wave vector disappears entirely on the other side of the CL-4i/CL-4ii boundary[22] in Fig. 1(a).

To make quantitative predictions for $CuFeO_2$ would require that we also include the interactions between adjacent hexagonal planes as well as the nontrivial effects of the scalene lattice distortion.[25] Nevertheless, the phase diagram of Fig. 2(b) provides some qualitative predictions for $CuFeO_2$. The thin solid curve indicates a possible trajectory through the phase diagram of Fig. 2(b) and accounts for the expected decrease[13,14] in the anisotropy with the magnetic field. The magnetization M and susceptibility $\chi = dM/dh$ along this curve are plotted in Figs. 3(a) to 3(d). As indicated on the right-hand side of Fig. 2, nine separate phase transitions are expected along this trajectory.

In agreement with Ref. 8, a canted 5-SL phase intercedes between the CNC and CL-5i phases. With either Al or Ga doping (corresponding to decreasing $D/|J_1|$), the NC-5i phase can supplant the CL-5i phase. Evidence for the NC-5i phase is provided by measurements on 2% Al-doped[5] and 3.5% Ga-doped[10] samples, where the magnetization M of the observed 5-SL phase increases linearly with the field. However, the predicted second-order transition between the NC-5i and CL-5i phases has not been seen. The NC-5i phase in pure $CuFeO_2$ might be eliminated by the scalene lattice distortion.[25]

Some evidence for the NC-3i phase was provided in Ref. 17, which observed that oxygen nonstoichiometry splits the 20 T transition from the CL-5i to the CL-3 phase into two transitions at 20 and 23 T, leaving room for the NC-3i phase between them. There is much stronger support for the predicted second-order transition from the CL-3 phase to the canted NC-3ii phase: both Terada *et al.*[13] and Lummen *et al.*[14] observed second-order transitions from the CL-3 to a canted phase at 34 T.

Lummen *et al.*[14] and Quiron *et al.*[15] observed a weakly first-order transition at either 53 or 49 T with $M \approx 0.65$. Figures 3(b) and 3(d) strongly suggest that this first-order transition occurs between the NC-3ii and SF-2 phases, with a predicted $M = 0.69$. Using the observed saturation field[16] of 70 T, we estimate that the even more weakly first-order transition from the SF-2 to the SF-1 phase will occur at about 65 T. Whereas the SF-1 phase has the wave vector $(0.85\pi,0)$ with a turn angle $\Delta\phi = 0.43\pi$ along the x direction, the SF-2 phase has the wave vector $(0.8\pi,0.43\pi)$ with a turn angle $\Delta\phi = 0.37\pi$ along the y direction.

The proximity of the CL-30 phase to the trajectory in Fig. 2(b) suggests that this phase may be accessible by oxygen nonstoichiometry, which is predicted to enhance the anisotropy.[17] The appearance of "exotic" 7-SL and 30-SL CL states[26] raises the possibility that even stranger CL states remain undiscovered. However, it is unlikely that any missing CL states will affect physical results along the trajectory plotted in Fig. 2(b).

Compelling evidence for the canted and SF phases requires future measurements. The NC-5i phase in doped $CuFeO_2$ should undergo a first-order transition to the NC-3i phase. The NC-5i and CL-5i phases can be distinguished by their inelastic neutron-scattering spectra: unlike the gapped excitations of the CL-5i phase, the spin excitations in the NC-5i phase are gapless due to rotational symmetry about the z axis. The transition from the SF-2 to the SF-1 phase might be detected by the small 2.4% drop in the susceptibility χ at about 65 T.

To conclude, the combination of MC simulations, spin-wave calculations, and variational techniques provides a powerful and efficient method for evaluating the magnetic

phase diagram of a frustrated magnet. Hopefully, the results of this paper will inspire future high-field measurements on $CuFeO_2$ and other frustrated magnets.

Research was sponsored by the US Department of Energy, Office of Basic Energy Sciences, Materials Sciences and Engineering Division (R.F.) and by the Center for Integrated Nanotechnologies, a US Department of Energy, Office of Basic Energy Sciences user facility at the Los Alamos National Laboratory, operated by the Los Alamos National Security, LLC, for the National Nuclear Security Administration of the US Department of Energy (J.H.). Computer time was provided by the Florida State University (G.B.).

[1]D. I. Khomskii, J. Magn. Magn. Mat. **306**, 1 (2006); S.-W. Cheong and M. Mostovoy, Nat. Mat. **6**, 13 (2007).

[2]G. Lautenschläger, H. Weitzel, T. Vogt, R. Hock, A. Böhm, M. Bonnet, and H. Fuess, Phys. Rev. B **48**, 6087 (1993); F. Ye, R. S. Fishman, J. A. Fernandez-Baca, A. A. Podlesnyak, G. Ehlers, H. A. Mook, Y. Wang, B. Lorenz, and C. W. Chu, *ibid.* **83**, 140401 (2011).

[3]S. Mitsuda, H. Yoshizawa, N. Yaguchi, and M. Mekata, J. Phys. Soc. Jpn. **60**, 1185 (1991).

[4]T. Kimura, J. C. Lashley, and A. P. Ramirez, Phys. Rev. B **73**, 220401(R) (2006).

[5]S. Kanetsuki, S. Mitsuda, T. Nakajima, D. Anazawa, H. A. Katori, and K. Prokes, J. Phys. Condens. Matter **19**, 145244 (2007).

[6]S. Seki, Y. Yamasaki, Y. Shiomi, S. Iguchi, Y. Onose, and Y. Tokura, Phys. Rev. B **75**, 100403(R) (2007).

[7]F. Ye, Y. Ren, J. A. Fernandez-Baca, H. A. Mook, J. W. Lynn, R. P. Chaudhury, Y.-Q. Wang, B. Lorenz, and C. W. Chu, Phys. Rev. B **78**, 193101 (2008).

[8]R. S. Fishman, Phys. Rev. Lett. **106**, 037206 (2011).

[9]N. Terada, T. Nakajima, S. Mitsuda, H. Kitazawa, K. Kaneko, and N. Metoki, Phys. Rev. B **78**, 014101 (2008).

[10]S. Seki, H. Murakawa, Y. Onose, and Y. Tokura, Phys. Rev. Lett. **103**, 237601 (2009).

[11]J. T. Haraldsen, F. Ye, R. S. Fishman, J. A. Fernandez-Baca, Y. Yamaguchi, K. Kimura, and T. Kimura, Phys. Rev. B **82**, 020404 (2010).

[12]S. Mitsuda, M. Mase, K. Prokes, H. Kitizawa, and H. A. Katori, J. Phys. Soc. Jpn. **69**, 3513 (2000).

[13]N. Terada, Y. Narumi, Y. Sawai, K. Katsumata, U. Staub, Y. Tanaka, A. Kikkawa, T. Fukui, K. Kindo, T. Yamamoto, R. Kanmuri, M. Hagiwara, H. Toyokawa, T. Ishikawa, and H. Kitamura, Phys. Rev. B **75**, 224411 (2007).

[14]T. T. A. Lummen, C. Strohm, H. Rakoto, A. A. Nugroho, and P. H. M. van Loosdrecht, Phys. Rev. B **80**, 012406 (2009).

[15]G. Quirion, M. L. Plumer, O. A. Petrenko, G. Balakrishnan, and C. Proust, Phys. Rev. B **80**, 064420 (2009).

[16]Y. Ajiro, T. Asano, T. Takagi, M. Mekata, H. A. Katori, and T. Goto, Physica B **201**, 71 (1994).

[17]M. Hasegawa, M. I. Batrashevich, T. R. Zhao, H. Takei, and T. Goto, Phys. Rev. B **63**, 184437 (2001).

[18]T. Takagi and M. Mekata, J. Phys. Soc. Japan **64**, 4609 (1995).

[19]M. E. Zhitomirsky and I. A. Zaliznyak, Phys. Rev. B **53**, 3428 (1996).

[20]R. S. Fishman and S. Okamoto, Phys. Rev. B **81**, 020402 (2010).

[21]M. Swanson, J. T. Haraldsen, and R. S. Fishman, Phys. Rev. B **79**, 184413 (2009); J. T. Haraldsen, M. Swanson, G. Alvarez, and R. S. Fishman, Phys. Rev. Lett. **102**, 237204 (2009).

[22]R. S. Fishman, J. Phys. Condens. Matter **23**, 366002 (2011).

[23]Because the NC-5ii phase of Ref. 8 is unstable, we have relabeled the NC-5iii phase as NC-5ii.

[24]J. T. Haraldsen and R. S. Fishman, J. Phys. Condens. Matter **21**, 216001 (2009).

[25]N. Terada, S. Mistuda, Y. Tanaka, Y. Tabata, K. Katsumata, and A. Kikkawa, J. Phys. Soc. Japan **77**, 054701 (2008).

[26]These exotic CL states also appear in the phase diagrams of Ref. 22 but do not affect its predictions for $CuCrO_2$.